Biointerface Research in Applied Chemistry
Open-Access Journal (ISSN: 2069-5837)

Article
Volume 13, Issue 5, 2023, 406
https://doi.org/10.33263/BRIAC135.406

Nanofluid Boundary Layer Analysis in the Presence of Magnetic Lines of Force Being Fixed Relatively to the Plate and the Water-based Nanofluid Containing Copper, Aluminum Trioxide, and Silicon Dioxide Nanoparticles

Rama Krishna Golla [1], Vijaya Kumar Avula Golla [1,*]

[1] Department of Mathematics, SAS, Vellore Institute of Technology, Vellore-632014, India; drveenavijayakumar@gmail.com (R.K); vijayakumarag@vit.ac.in (V.K.A.G);
* Correspondence: vijayakumarag@vit.ac.in (V.K.A.G.);

Scopus Author ID 57696411400
Received: 30.07.2022; Accepted: 20.09.2022; Published: 17.11.2022

Abstract: An exact solution to the problem of effects of generation or absorption and natural convective magnetic nanofluid flow past an upright plate, in a case where the magnetic lines are aligned to the plate or the fluid magnetic lines are being associated with liquid (i.e., K=0) and these magnetic force of flux being associate with the plate (i.e., K=1) are investigated. Three types of water-heat transfer-based nanofluids containing copper, aluminum oxide, and titanium dioxide are taken. The dimensionless governing equations involved in the present analysis are tackled with the help of integral transforms. For plotting figures and tables, numerical values are computed for Nanofluid velocity, temperature, heat, and mass flow rates near the adjacent plate boundary.

Keywords: exact solution; magnetic nanofluid; natural convective heat transfer; heat transmission rate; boundary layer of the ionosphere.

1. Introduction

The study of heat transfer has attracted many researchers and Gained remarkable attention in the modern era—several engineering processes like transmission of energy in coolant desert towers in water body's surface evaporations. Few applications can be found in manufacturing industries, such as in the electric and power generation industries. One application can be used to generate electricity by extracting power from the motion of the conductive liquid. In moving liquids, the study involves heat generation or absorption, which is most significant in dissociated chemically reacting fluids. The impact of the heat source may change the energy distribution so that further it leads to nuclear reactor particle decomposition, computer chips, and in preparation of semiconductor materials, viz., silicon crystalline used in engineering fabrication of IC circuits, liquid type solar cells, and conventional photo-voltaic. Since few liquids and gases in nature tend to absorb and emit radiation, the fluid temperature distribution and heat flow rate is essential in the presence of a magnetic field because the heat transmission by linear radiation attains a greater impact in concern of some space engineering and higher order temperature applications.

Hence, heat transfer by thermal radiation is becoming of greater importance when we are concerned with space applications and higher operating temperatures. Nanofluids are

nanotechnology-based heat transfer fluids that are derived by stably suspending nanometer-sized particles in conventional heat transfer fluids. Choi [1] first introduced the phrase of nanofluid prepared by solid-type nanoparticles immersed in a liquid. Common fluids say ethylene glycol, water, engine oils, etc., configure significantly low thermal conductivity. The works done experimentally by Eastman *et al*. [2] examined that a Nanofluid prepared with copper metal nanoparticles suspended in a liquid shown that about 60 percent growth in thermal conductivity. Besides that, it is reported that there is high thermal conductivity if it is the Nanofluid with similar nanoparticles with the replacement of base fluid, either pure ethylene glycol or ethylene glycol. There is a 40 percent improvement in thermal conductivity in a Nanofluid prepared by ethylene glycol around 0.003 volume fraction and copper nanoparticles with a radius of five centimeters as determined by Eastman *et al.* [3] and Choi *et al*. [4]. Previous theoretical studies by Das *et al*. [5] indicated that particle shape significantly affects effective nanofluid thermal conductivity, but particle size and thermal conductivity had little effect. Keblinski *et al*. [6] investigated how nanoparticle suspensions' dispersion patterns affected heat transfer. Buongiorno [7] studied energy transmission and flow pattern implications of a nanoliquid along a stretchable exponential sheet. Nanoliquid heat transmission rate is supervised through their review articles by Das and Choi [8]. The thermophoresis nanoliquid properties such as density, heat capacity, and viscosity vary with base fluids, which significantly improves heat flow rate through excess heat conductivity, as reported by Kakac and Pramuanjaroenkij [9]. Heat transmission rate and thermal conduciveness can be improved significantly with the suspension of nanoparticles such as fluids in engine oil, seawater, and a mixer of ethylene glycol. The topic of heat transfer in nanofluids has been surveyed in review articles by Wang and Mazumdar [10], Sheikholeslami *et al*. [11], Sheikholeslami [12], and Kandelousi [13].

The study of Magneto hydrodynamics with heat transfer in the presence of radiation and diffusion has attracted the attention of many researchers due to its diverse applications. In astrophysics and geophysics, it is applied to study stellar and solar structures, radio propagation by the ionosphere, etc. It is concerned with the interaction of electrically conducting fluids and electromagnetic fields. When a conducting fluid moves through a magnetic field, an electric field and, consequently, a current may be induced, and in turn, the current interacts with the magnetic field to produce a body force on the fluid. Such interactions occur both in nature and in new artificial devices. In the laboratory, many new devices have been made that utilize the MHD interaction directly, such as propulsion units and power generators, or involve fluid electromagnetic field interactions, such as electron beam dynamics, traveling wave tubes, electrical discharges, MHD pumps, MHD bearing, etc. Kuznetsov and Nield [14] The Nanofluid flow through natural convection along a boundary of an upright plate. Hamad and Pop [15] Examined hydro magnetic Nanofluid unsteady flow along a porous flat plate under uniform heat generation in a revolving frame reference. Hamad *et al*. [16] Hamed *et al*. [16] scrutinized the impact of uniform strength magnetic field over a Nanofluid by a natural convection process along a boundary of a semi-infinite upright plate of a conductive Nanofluid boundary layer flow consisting of a pure liquid with nanosized particles along a porous upright plate under the influence of magnetic induction with heat sources and injecting effects. By incorporating the impact of Brownian motion with thermophoresis, a model developed on Nanofluid has been studied by Chamkha and Aly [17]. Turkyilmazoglu and Pop [18] Heat mass flow rates over a conductive radiated Nanofluid are considered along an upright plate. Turkyilmazoglu [19] has obtained a Heat mass flow of Magnetic Nanofluid slip flow In the

presence of a fixed magnetic field with respect to the fluid or the plate, Rushi Kumar *et al*. [20] studied the effects of thermal diffusion and radiation on unsteady free convection flow. Sheikholeslami *et al*. [21] investigated the impact of linear radiation and thermal diffusion on a magnetic Nanofluid flow and the heat transmission rate by means of a two-phase model. Sheikholeslami *et al*. [22 The analytical solutions using the Lattice-Boltzmann method over a conductive magnetic Nanofluid flow presented by Sheikholeslami *et al*. [23]. Sheikholeslami and Ganji [24] scrutinized the impact of magnetic effect and energy transmission over an unsteady flow of Nanofluid. Das and Jana [25] have analyzed Nanoliquid magnetic flow and heat transmission by linear radiation over the edge of an upright plate with the popular integral transforms technique. Loganathan *et al*. [26] analyzed conductive nanofluid flow over the boundary of an upright plate influenced by energy generation. Ajay Kumar Sing [27] studied the effects of heat source/sink and radiative heat transfer on hydromagnetic natural convection flow through a vertical channel. Some studies involving MHD with nanofluid are cited in the references [28-50].

However, in the literature, we found less attention was paid to studying Convective Nanofluid flow along the edge of an upright plate influenced by the magnetic force field by considering the field of force aligned either with fluid or to the plate. Three varieties of liquid-based nanofluids prepared by nanoparticles of Titanium dioxide, Aluminium trioxide, and copper metal are taken. They obtained an exact solution with the help of the transforms method, and the numerical results were computed with the approximated error functions that appeared in the solution.

2. Mathematical Analysis

Conductive Nanofluid unsteady flow and energy transmission bounded by impulsively rolling plate with fixed temperature influenced by the magnetic field when the force field is oriented with the fluid or to the plate as a dual case (1) when the force field is oriented towards the fluid, i.e. (K=0) and when force field is oriented towards to the plate, i.e. (K=1) have been considered. Through the plate in the perpendicular positive x-direction, and y-axis is taken normal to it in the direction of the applied transverse magnetic field. At the initial time, the plate and surrounding fluid in the plane have equal temperatures in a stationary condition for all the points in the entire flow region $y \geq 0$. At the time $t \geq 0$, In its preserve plane, the plate motion is $u = \lambda u_0$ in the upward direction. At the same time, the edge temperature is elevated T_w. A transverse magnetic field of uniform strength B_0 is assumed to be applied normally to the plate. The gradient of pressure is ignored in the momentum equation, and applied a linear radiative heat flux across the flow direction. This study considered distinct nanofluids, namely metals copper, Aluminium trioxide, and Titanium oxide. And further, it is considered base liquid water and nanoparticles maintained equilibrium. The thermal physical properties of the nanofluids are given in Table 1. For free convection flow, it is also assumed that 1) The induced magnetic field is assumed to be negligible as the magnetic Re of the flow is taken to be very small. 2) The viscous dissipation is neglected in the energy equation. 3) The effects of variation in density (ρ) with temperature considered only on the body force term, in accordance with the usual Boussinesq approximation. 4) The fluid considered here is gray, absorbing/emitting radiation but a non-scattered medium. 5) Since the flow of the fluid is assumed to be in the

direction of $x-$ axis, so the physical quantities are functions of the space co-ordinate y and t only.

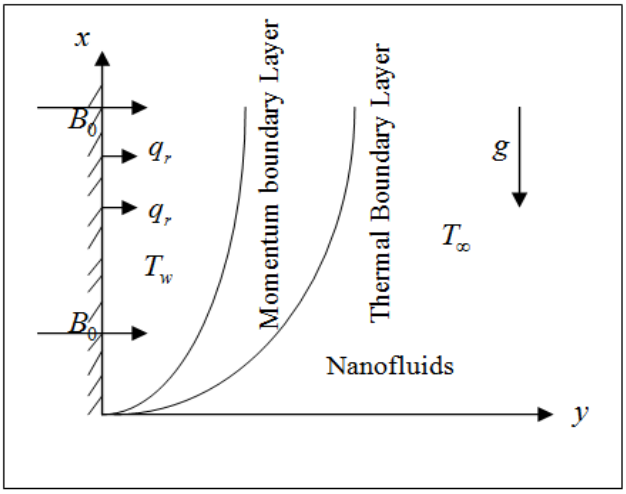

Figure 1. Physical coordinate system.

The flow is governed by the following equations:

$$\rho_{nf}\frac{\partial u}{\partial t}=\mu_{nf}\frac{\partial^2 u}{\partial y^2}+g(\rho\beta)_{nf}(T-T_\infty)-\sigma_{nf}B_0^2u \tag{2.1}$$

$$(\rho c_p)_{nf}\frac{\partial T}{\partial t}=k_{nf}\frac{\partial^2 T}{\partial t^2}-\frac{\partial q_r}{\partial y}-Q_0(T-T_\infty) \tag{2.2}$$

If the magnetic field is fixed relative to the plate, the momentum equation (1) is replaced by (see Cramer [51], Raptis [52], and Tokis [53]):

$$\rho_{nf}\frac{\partial u}{\partial t}=\mu_{nf}\frac{\partial^2 u}{\partial y^2}+g(\rho\beta)_{nf}(T-T_\infty)-\sigma_{nf}B_0^2\left[u-u_0f\left(t'\right)\right] \tag{2.3}$$

Combining (2.1) and (2.3):

$$\rho_{nf}\frac{\partial u}{\partial t}=\mu_{nf}\frac{\partial^2 u}{\partial y^2}+g(\rho\beta)_{nf}(T-T_\infty)-\sigma_{nf}B_0^2\left[u-Ku_0f\left(t'\right)\right] \tag{2.4}$$

where $K=\begin{cases}0 \text{ if } B_0 \text{ is fixed relative to the fluid}\\ 1 \text{ if } B_0 \text{ is fixed relative to the plate}\end{cases}$

for an exponentially accelerated plate, $f\left(t'\right)=\exp\left(a_0't'\right)$, where a_0' is the dimensional acceleration; where u is the velocity components along the x-direction, Q_0 heat generation constant, T-nanofluid temperature, μ_{nf} nanofluid viscocity, β_{nf} nanofluid thermal coefficnet, ρ_{nf} nanofluid mass desnsity, σ_{nf} nanofluid electgricity, k_{nf} nanofluid heat conductivity, g is the gravity, q_r linear radiative heat flux and $(\rho c_p)_{nf}$ nanofluid thermal capacitance which are given by:

$$\mu_{nf}=\frac{\mu_f}{(1-\phi)^{2.5}},\ \rho_{nf}=(1-\phi)\rho_f+\phi\rho_s,\ (\rho c_p)_{nf}=(1-\varphi)(\rho c_p)_f+\phi(\rho c_p)_s,\ \sigma=\frac{\sigma_s}{\sigma_f},$$

$$(\rho\beta)_{nf}=(1-\phi)(\rho\beta)_f+\phi(\rho\beta)_s,\ \sigma_{nf}=\sigma_f\left[1+\frac{3(\sigma-1)\phi}{(\sigma+2)-(\sigma-1)\phi}\right], \tag{2.5}$$

where ϕ, ρ_f, ρ_s, σ_f, σ_s, μ_f, $(\rho c_p)_f$ $(\rho c_p)_s$ are respectively the volume ratio, density, electrical conductivity, viscocity ofthe heat capacitance of the nanoparticle and base

fluid. The effective thermal conductivity of the nanofluid for spherical nanoparticles is given by Hamilton and Crosser's model, followed by Kakac and Pramuanjaroenkij [9], and Oztop and Abu-Nada [54] is given by:

$$k_{nf} = k_f \left[\frac{k_s + 2k_f - 2\phi(k_f - k_s)}{k_s + 2k_f + \phi(k_f - k_s)} \right] \tag{2.6}$$

where k_f and k_s the thermal conductivity of the fluid and nanoparticles. In Eqs. (2.1) to (2.6), the subscripts nf, f and s respectively Nanofluid thermophoresis properties of nanofluid, base liquid, and nanometer particles with associated initial and conditions defined at boundaries are

$$t \le 0 : u = 0, \qquad T = T_\infty, \qquad \text{for all} \quad y \ge 0$$
$$t > 0 : u = \lambda u_0, \qquad T = T_w \qquad \text{at} \quad y = 0$$
$$u \to 0, \quad T \to T_\infty, \qquad as \quad y \to \infty$$

where λ denotes the direction of motion of the plate with λ =0 for the stationary plate, while $\lambda = \pm 1$ for the fourth and back motion of the plate. Plate momentum. Since the liquid is thick optically (free path least mean of the photon) gray gas (which have the nature of receiving and omitting radiation) for such medium, the characteristic length is very less in comparison with the penetration distance of linear radiation. For an optically thick fluid, we can adopt Rosseland [27] approximation applies to optically thick media and gives the net radiation heat flux q_r by the expression:

$$q_r = -\frac{4\sigma^*}{3k^*}\frac{\partial T^4}{\partial y} \tag{2.7}$$

where $\sigma^* (= 5.67 \times 10^{-8} W/m^2K^4)$ Stefan-Boltzmann coefficient while km^{-1} is the mean value of absorbing coefficient in Rossonold approximation. Since natural convection gives very low variations in temperature inside the flow regime, hence it is to be considered only the first term in Taylor's series as a linear function in temperature. The detailed procedure is given here:

$$T^4 = T_\infty^4 + 4T_\infty^3(T - T_\infty) + 6T_\infty^2(T - T_\infty)^2 + --- \tag{2.8}$$
$$T^4 \cong T_\infty^4 + 4T_\infty^3(T - T_\infty)$$
$$T^4 \cong T_\infty^4 + 4TT_\infty^3 - 4T_\infty^4$$
$$T^4 \cong 4TT_\infty^3 - 3T_\infty^4 \tag{2.9}$$

On the use of Eqs. (2.7) and (2.9), Eq. (2.5) becomes:

$$\frac{\partial T}{\partial t} = \frac{1}{(\rho c_p)_{nf}} \left[\left(k_{nf} + \frac{16\sigma^* T_\infty^3}{3k^*} \right) \frac{\partial^2 T}{\partial y^2} - Q_0(T - T_\infty) \right] \tag{2.10}$$

Introducing non-dimensional variables:

$$\eta = \frac{u_0 y}{\nu_f}, \ \tau = \frac{u_0^2 t}{\nu_f}, \ U = \frac{u}{u_0}, \ \theta = \frac{T - T_\infty}{T_w - T_\infty}, \ t = \frac{t' u_0^2}{\nu}, \ a_0 = \frac{a'\nu}{u_0^2}, \ Q = \frac{Q_0 \nu_f}{u_0^2 (\rho c_p)_f} \tag{2.11}$$

We get the following governing equations which are dimensionless:

$$\frac{\partial U}{\partial \tau} = a_1 \frac{\partial^2 U}{\partial \eta^2} + Gra_2\theta - M^2 a_3(u_0 - Ke^{a_0 t}) \tag{2.12}$$

$$\frac{\partial \theta}{\partial \tau} = a_4 \frac{\partial^2 \theta}{\partial \eta^2} + a_5 \theta \tag{2.13}$$

where:

$$x_1 = \left[(1-\phi) + \phi \left(\frac{\rho_s}{\rho_f} \right) \right],\ x_2 = \left[(1-\phi) + \phi \frac{(\rho\beta)_s}{(\rho\beta)_f} \right],\ x_3 = \left[(1-\phi) + \phi \frac{(\rho c_p)_s}{(\rho c_p)_f} \right],$$

$$x_4 = \left[\frac{k_s + 2k_f - 2\phi(k_f - k_s)}{k_s + 2k_f + \phi(k_f - k_s)} \right],\ x_5 = \left[1 + \frac{3(\frac{\sigma_s}{\sigma_f} - 1)\phi}{(\frac{\sigma_s}{\sigma_f} + 2) - (\frac{\sigma_s}{\sigma_f} - 1)\phi} \right],\ a_1 = \frac{1}{(1-\phi)^{2.5} x_1},$$

$$a_2 = \frac{x_2}{x_1},\ a_3 = \frac{x_5}{x_1},\ a_4 = \frac{1}{x_3 \,\mathrm{Pr}}(x_4 + Nr),\ a_5 = \frac{-Q}{x_3} \tag{2.14}$$

and $M^2 = \sigma_f B_0^2 \nu_f / \rho_f u_0^2$, is the magnetic parameter, $Nr = 16\sigma^* T_\infty^3 / 3k_f k^*$ the radiation parameter, $\mathrm{Pr} = \mu_f c_p / k_f$ is Prandtl number, and $Gr = g\beta_f \nu_f (T_w - T_\infty) / u_0^3$ the Grashof number. The magnetic parameter (M^2) is the ratio of electromagnetic force to viscous force. Grashof number (Gr) that approximates the ratio of the buoyant force to the viscous force acting. Prandtl number (Pr) is defined as the quotient of the momentum diffusivity to thermal diffusivity. Large Nr signifies a large radiation effect while $Nr \to 0$ corresponding to a zero radiation effect.

The initial and boundary conditions in the dimensionless form are as follows:

$$\begin{aligned} &t \le 0 : U = 0, \quad \theta = 0, \quad \text{for all} \quad \eta \ge 0 \\ &t > 0 : U = \lambda, \quad \theta = 1, \quad \text{at} \quad \eta = 0 \\ &U \to 0, \quad \theta \to 0, \quad as \quad \eta \to \infty \end{aligned} \tag{2.15}$$

The appeared physical parameters are defined in the nomenclature. The dimensionless governing equations form (2.12) and (2.13), subject to the boundary conditions (2.15), are solved by the usual Laplace transform technique, and the solutions are expressed in terms of exponential and complementary error functions:

$$\theta(\eta,\tau) = \frac{1}{2}\left(\exp\left(\eta\sqrt{d_0}\right) erfc\left(\frac{\eta}{2\sqrt{a_4 t}} + \sqrt{d_0 t} \right) + \exp\left(-\eta\sqrt{d_0}\right) erfc\left(\frac{\eta}{2\sqrt{a_4 t}} - \sqrt{d_0 t} \right) \right) \tag{2.16}$$

$$U(\eta,\tau) = \frac{(\lambda - d_2)}{2}\left[\exp(y\sqrt{d_1}) erfc\left(\frac{\eta}{2\sqrt{\tau}} + \sqrt{d_1\tau} \right) + \exp(-y\sqrt{d_1}) erfc\left(\frac{\eta}{2\sqrt{\tau}} - \sqrt{d_1\tau} \right) \right]$$

$$+ \frac{d_5 e^{-d_3\tau}}{2}\left[\exp(y\sqrt{d_7}) erfc\left(\frac{\eta}{2\sqrt{\tau}} + \sqrt{d_7\tau} \right) + \exp(-y\sqrt{d_7}) erfc\left(\frac{\eta}{2\sqrt{\tau}} - \sqrt{d_7\tau} \right) \right]$$

$$- \frac{d_6 e^{a_0\tau}}{2}\left[\exp(y\sqrt{d_1 + a_0}) erfc\left(\frac{\eta}{2\sqrt{\tau}} + \sqrt{(d_1 + a_0)\tau} \right) + \exp(-y\sqrt{d_1 + a_0}) erfc\left(\frac{\eta}{2\sqrt{\tau}} - \sqrt{(d_1 + a_0)\tau} \right) \right]$$

$$+ d_6 e \exp(-d_1\tau) erfc\left(\frac{\eta}{2\sqrt{\tau}}\right)$$

$$+\frac{d_5}{2}\left[\exp(\eta\sqrt{d_0})erfc\left(\frac{\eta}{2\sqrt{a_4\tau}}+\sqrt{d_0\tau}\right)+\exp(-\eta\sqrt{d_0})erfc\left(\frac{\eta}{2\sqrt{a_4\tau}}-\sqrt{d_0\tau}\right)\right]$$

$$-\frac{d_5 e^{-d_3\tau}}{2}\left[\exp(\eta\sqrt{d_8})erfc\left(\frac{\eta}{2\sqrt{a_4\tau}}+\sqrt{d_8\tau}\right)+\exp(-\eta\sqrt{d_8})erfc\left(\frac{\eta}{2\sqrt{a_4\tau}}-\sqrt{d_8\tau}\right)\right]+d_6\exp(a_0\tau)$$

$$-d_6\exp(-d_1\tau) \tag{2.17}$$

where:

$$d_0=\frac{-a_5}{a_4},\quad d_1=a_3M^2,\quad d_2=\frac{-Gra_2a_4}{1-a_4},\quad d_3=\frac{d_1a_4-a_5}{1-a_4},\quad d_4=M^2a_3K,\quad d_5=\frac{d_2}{d_3},$$

$$d_6=\frac{d_4}{a_0+d_1}$$

$$d_7=(d_1+d_3),\ d_8=\frac{(d_3-a_5)}{a_4}$$

2.1. Skin-friction.

From the velocity field, we study the skin friction (rate of change of velocity at the plate), which is given in non-dimensional form as follows:

$$C_f=-\left[\frac{dU}{d\eta}\right]_{\eta=0} \tag{2.18}$$

From Eqs. (2.17) and (2.18), we get skin friction as follows:

$$C_f=(\lambda-d_5)\left(-\sqrt{d_1}erf\left(\sqrt{d_1\tau}\right)+\frac{e^{-d_1\tau}}{\sqrt{\pi\tau}}\right)\qquad+d_5\exp(-d_3\tau)\left(\frac{e^{-d_7\tau}}{\sqrt{\pi\tau}}-\sqrt{d_7}erf\left(\sqrt{d_7\tau}\right)\right)$$

$$+d_6\exp(a_0\tau)\left(-\frac{e^{-(d_1+a_0)\tau}}{\sqrt{\pi\tau}}+\sqrt{d_1+a_0}erf\left(\sqrt{(d_1+a_0)\tau}\right)\right)\qquad+\frac{d_6e^{-d_1\tau}}{\sqrt{\pi\tau}}$$

$$-d_5\left(-\frac{e^{-d_0\tau}}{\sqrt{\pi a_4\tau}}+\sqrt{d_0}erf\left(\sqrt{d_0\tau}\right)\right)+d_5\exp(-d_3\tau)\left(-\frac{e^{-d_8\tau}}{\sqrt{\pi a_4\tau}}+\sqrt{d_8}erf\left(\sqrt{d_8\tau}\right)\right) \tag{2.19}$$

2.2. Nusselt Number.

From the temperature field, we study the Nusselt number (rate of change of velocity at the plate), which is given in non-dimensional form as follows:

$$Nu=-\left[\frac{d\theta}{d\eta}\right]_{\eta=0} \tag{2.20}$$

From Eqs. (2.16) and (2.20), we get the Nusselt number as follows:

$$Nu=\frac{e^{-d_0\tau}}{\sqrt{\pi a_4\tau}}-\sqrt{d_0}erf\left(\sqrt{d_0\tau}\right) \tag{2.21}$$

3. Results and discussion

In order to get a clear insight into the physical problem, fluid momentum, fluid temperature, rate of energy flow, and the friction drag very closer to the plate have been discussed by the numerical values for the parameters like a magnetic parameter M^2, radiation parameter Nr, volume fraction parameter ϕ, time τ, heat source parameter Q and thermal Grashof number Gr in Figures 2-25. The values of the volume fraction of nanoparticles are taken in the range of $0 \le \phi \le 0.2$. The case M^2 =0 corresponds to the absence of a magnetic field and $\phi = 0$ for regular fluid. The velocity profiles are presented in Figures 2 to 13 when the magnetic field associated with the fluid (K=0) is deliberated in case (i) and the magnetic field is aligned through the plate (K=1) revealed in case (ii).

The effects of nanoparticles, M^2, ϕ, Nr, τ and Gr on the velocity field is illustrated in Figure 2 to13 in the presence of radiation parameter when other parameters are fixed. Figure 2 it is we observe that the velocity distribution for Al_2O_3 –water and TiO_2- water are the same as their densities, but due to the high density of Cu, Cu- water, the dynamic viscosity increases more, leading to a thinner boundary layer than other particles in the case of the fixed plate ($\lambda = 0$) and as well as a moving plate ($\lambda = \pm 1$). Figure 3 reveals that the velocity of nanoparticles at the plate decreases due to the reduction of momentum of the boundary layer of nanoparticles. Due to the heat transfer, a number of charges are generated within the copper than the rest of the particles. We found that the velocity of Cu nanoparticles increases while its viscosity decreases than other particles in the case of the fixed plate ($\lambda = 0$) and as well as a moving plate ($\lambda = \pm 1$). Figure 4 depicts that with increasing magnetic parameters, the momentum of boundary layer thickness decreases, and consequently, it accelerates the viscosity of the fluid. Therefore, it decreases the velocity of the fluid. Figure 5 noticed that the fluid velocity accelerates increasing values of M^2. The momentum boundary layer thickness increases for increasing values of M^2 for the case of the fixed plate ($\lambda = 0$) and as well as a moving plate ($\lambda = \pm 1$). Figure 6 reveals the effect of the solid volume fraction of nanoparticles on the fluid velocity. The fluid velocity increases for the increasing values of volume fraction for the case of the fixed plate ($\lambda = 0$) and as well as a moving plate ($\lambda = \pm 1$). Figure 7 displays the effect of the volume fraction of nanoparticles on the fluid velocity increases due to the absence of surface tension forces and viscosity for the case of the fixed plate ($\lambda = 0$) and as well as a moving plate ($\lambda = \pm 1$). In Figure 8 and Figure 9, the fluid velocity decreases with the value of radiation parameter Nr increases for both cases of the fixed plate ($\lambda = 0$) and as well as a moving plate ($\lambda = \pm 1$). Also, it noted that the momentum of boundary layer thickness decreases when Nr tends to increase inside a boundary layer region, and consequently, it accelerates the viscosity of the fluid. Figure 10 shows that the velocity decreases with the increase of time owing to the decrease of energy in the displacement of fluid for the case of the fixed plate ($\lambda = 0$) and as well as a moving plate ($\lambda = \pm 1$).

Figure 11 depicts that velocity rises over time in the presence of a heat source due to the fact that in both the situation of a stationary plate ($\lambda = 0$) and a moving plate ($\lambda = \pm 1$), the nanoparticles in the plate. Figure 12 and Figure 13 The heat source parameter increases, and more heat is produced due to the fact that nanofluid velocity increases for the case of the fixed plate ($\lambda = 0$) and as well as a moving plate ($\lambda = \pm 1$).

The behavior of fluid temperature by the influence of radiation parameter, Prandtl number heat sour/sink parameter, time, and volume fraction are illustrated in Figures 14-19. Figure 14 shows the variations for the three types of water-based nanofluids Cu-water, Al_2O_3-

water, and TiO_2 – water. However, due to higher thermal conductivity than Al_2O_3-water and TiO_2 – water nanofluids. It is also observed that the thermal boundary layer thickness is more for Cu- water than Al_2O_3-water and TiO_2 – water. Figure 15 and Figure 16 it is observed that the effect of the volume fraction of nanoparticles and the radiation parameter of the temperature distribution. Metallic nanoparticles have much higher heat conductivity than common liquids. It also observed that the thermal boundary layer increased with nanoparticle volume fraction. It is observed that the fluid temperature increases as Nr increments due to the fact the conduction effect of the nanofluid increases in the presence of thermal radiation. Therefore, higher values of radiation parameters incriminate higher surface heat flux and increase the temperature within the boundary layer region. It also observed that thermal boundary layer thickness increases with Nr increasing values. Figure 17 reveals that the temperature of the flow field decreases in magnitude as Pr increases. This is due to the fact that a higher Prandtl number fluid has a relatively low thermal conductivity, which reduces conduction and the thermal boundary layer thickness, and as a result, temperature decreases. Figure 18 depicts the temperature increases with increasing time. In figure 19 increasing the value of the heat source/sink tends to decrease the fluid's thermal state. In turn, a decrease in the fluid temperature induces a flow toward the plate through the thermal buoyancy effect. It is seen that from Figure 20 Nusselt number increases with increasing radiation parameter Nr. Figure 21 reveals that the Nusselt number increase with decreasing the Prandtl number. The reason is that small Pr values are equivalent to increasing the thermal conductivity, and therefore heat can diffuse away from the plate more rapidly than higher Pr values. Hence the rate of heat transfer is reduced. In general Prandtl number for water is higher than for air. Figure 22 and Figure 23 illustrate that the rate of change of velocity of nanoparticles at the plate decreases due to the reduction of momentum of the boundary layer of nanoparticles.

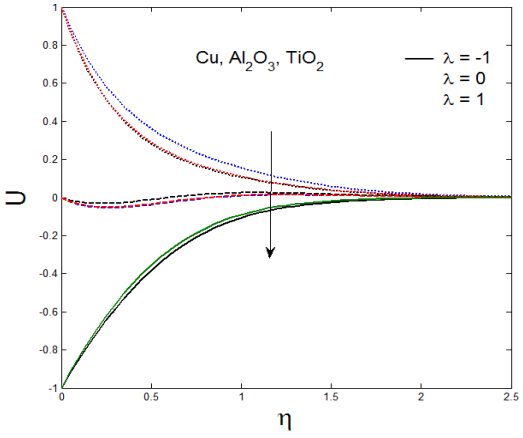

Figure 2. Velocity profile for different nanofluids when *K*=0.

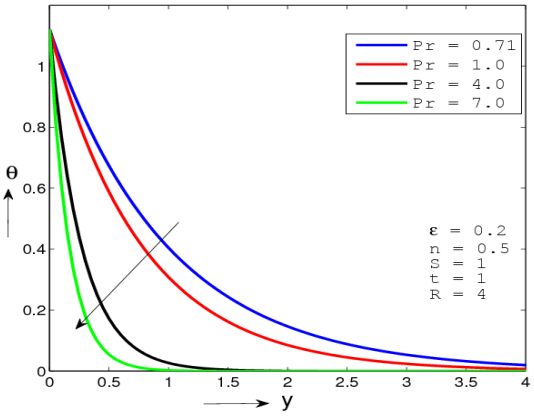

Figure 3. Temperature profiles for various values of *Pr*.

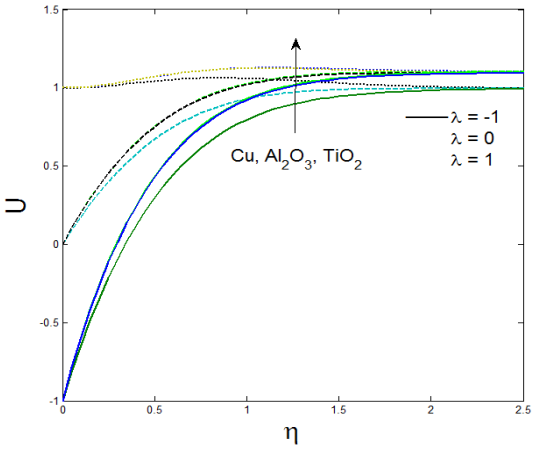

Figure 4. Velocity profile for different nanofluids when *K*=1.

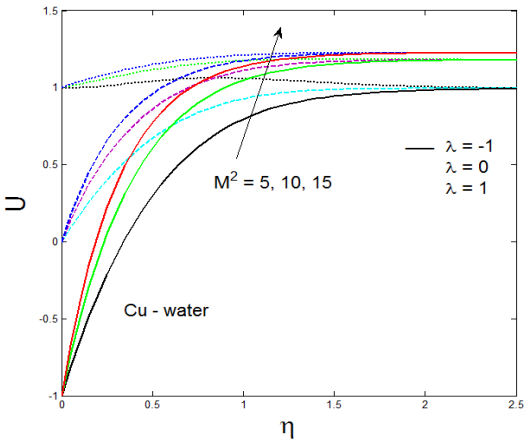

Figure 5. Velocity profile for different M^2 when *K*=1.

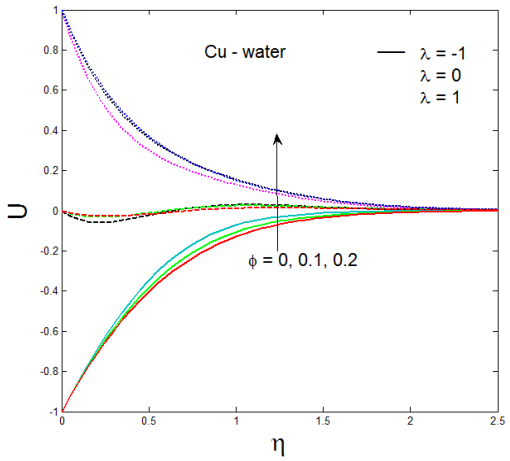

Figure 6. Velocity profile for different ϕ when *K*=0.

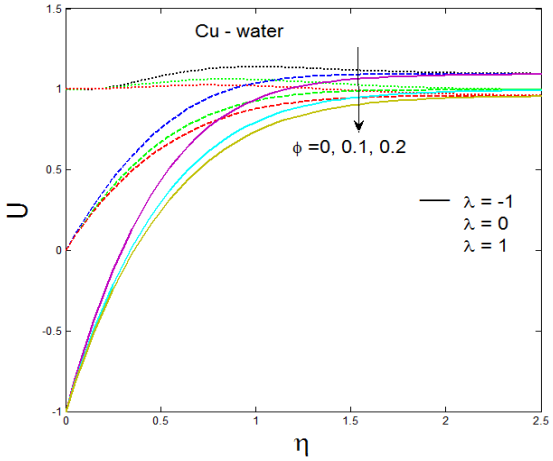

Figure 7. Velocity profile for different ϕ when *K*=1.

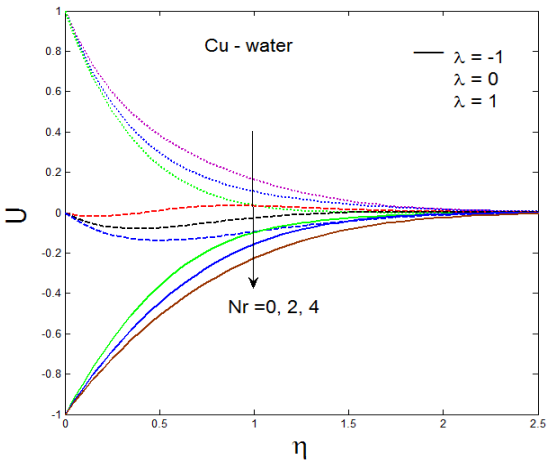

Figure 8. Velocity profile for different *Nr* when *K*=0.

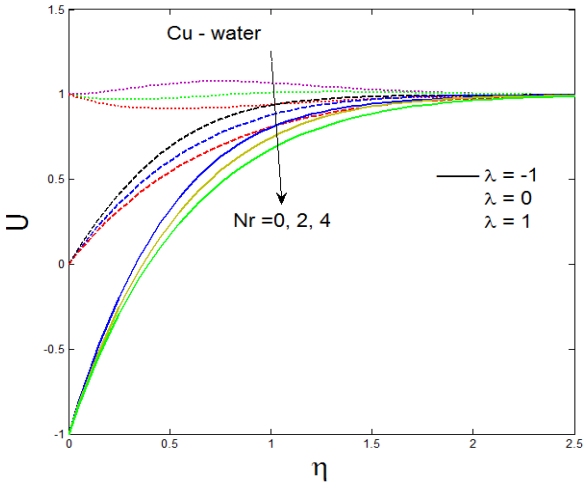

Figure 9. Velocity profile for different *Nr* when *K*=1.

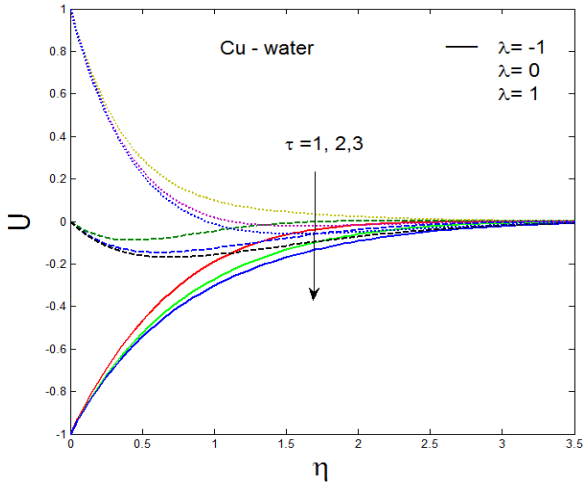

Figure 10. Velocity profile for different τ when *K*=0.

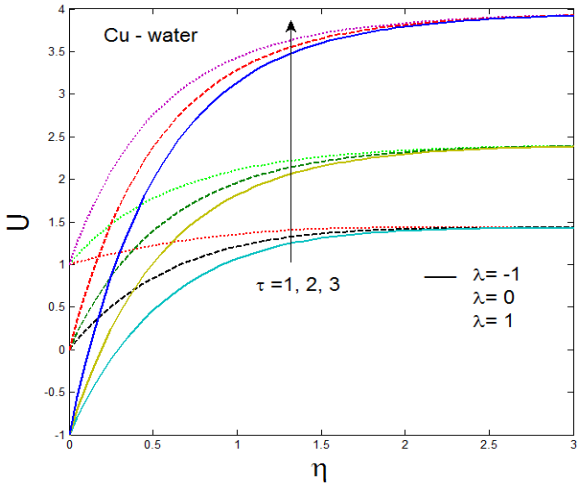

Figure 11. Velocity profile for different τ when *K*=1.

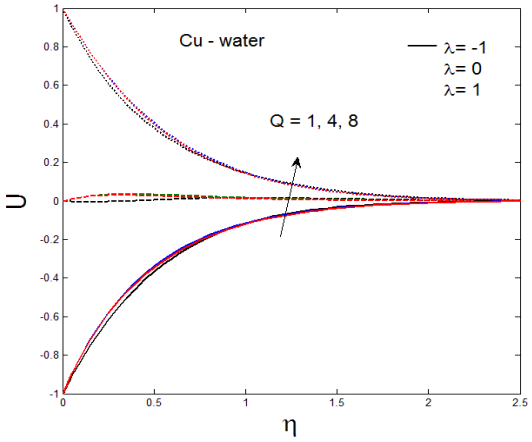

Figure 12. Velocity profile for different *Q* when *K*=0.

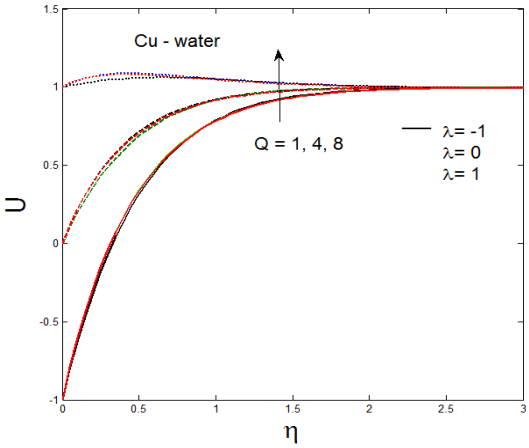

Figure 13. Velocity profile for different *Q* when *K*=1.

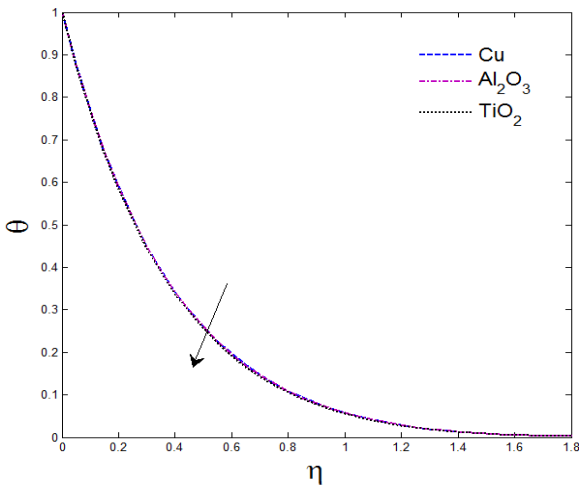

Figure 14. Temperature profile for different nanofluids when Nr =0.5, ϕ =0.1, and *Pr* =6.2.

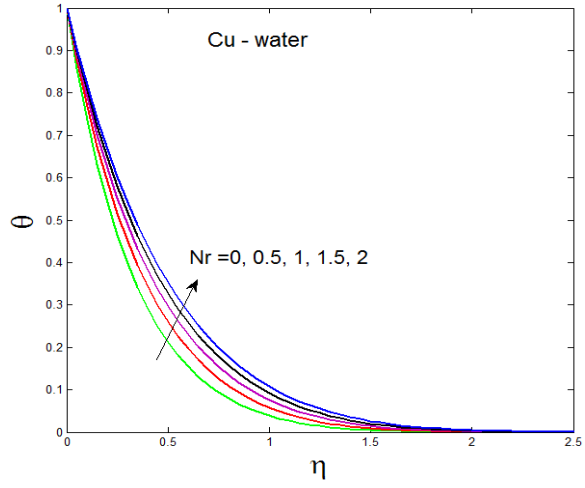

Figure 15. Temperature profile for different *Nr* when ϕ =0.1, *Pr*=6.2, *Q*=0.2 and τ =0.5.

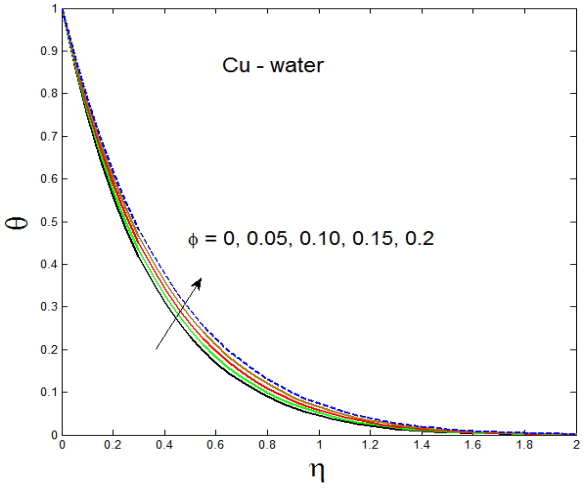

Figure 16. Temperature profile for different ϕ when Nr =0.5, Pr =6.2 Q=0.2 and τ =0.5.

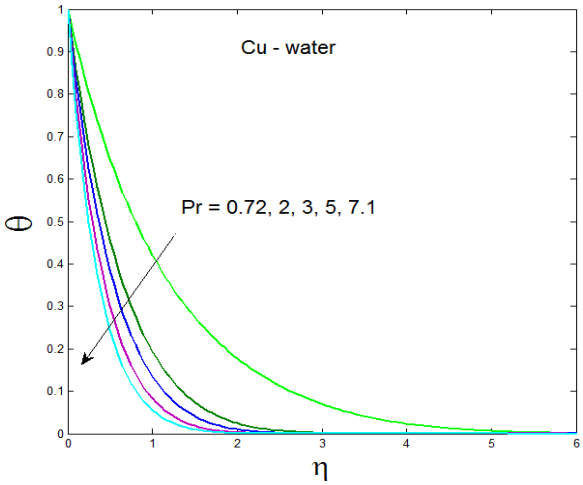

Figure 17. Temperature profile for different Pr when Nr =0.5, ϕ =0.1, Q =0.2 and τ =0.5.

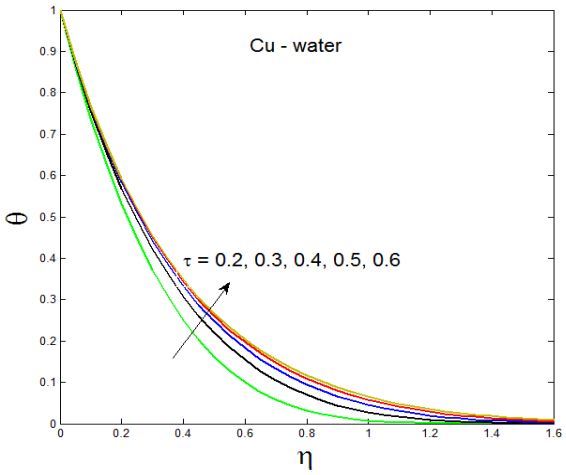

Figure 18. Temperature profile for different τ when Nr =0.5, ϕ =0.1, Q=0.2 and Pr =6.2.

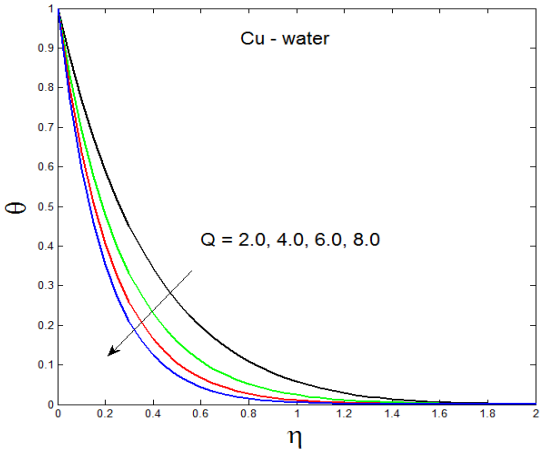

Figure 19. Temperature profile for different Q when Nr =0.5, Pr=6.2 and τ =0.5.

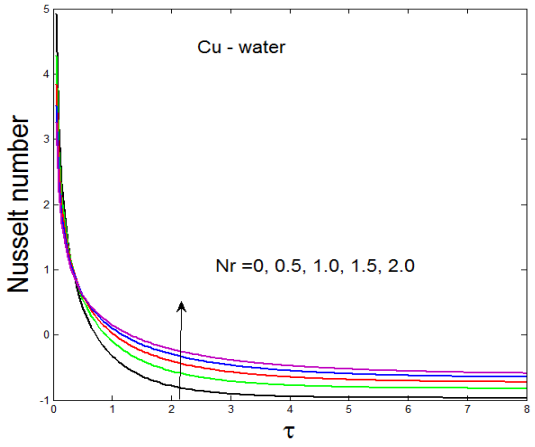

Figure 20. Nuselt number for different Nr.

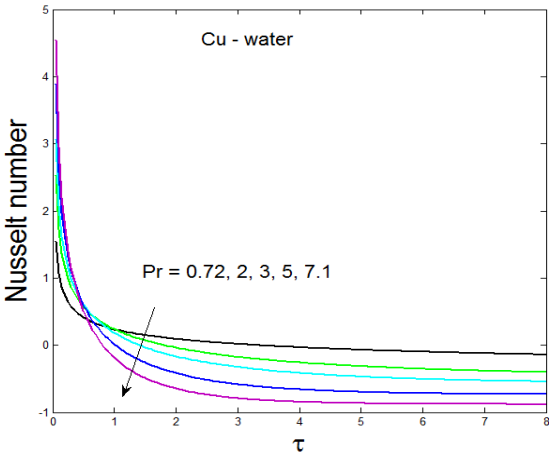

Figure 21. Nuselt number for different Pr.

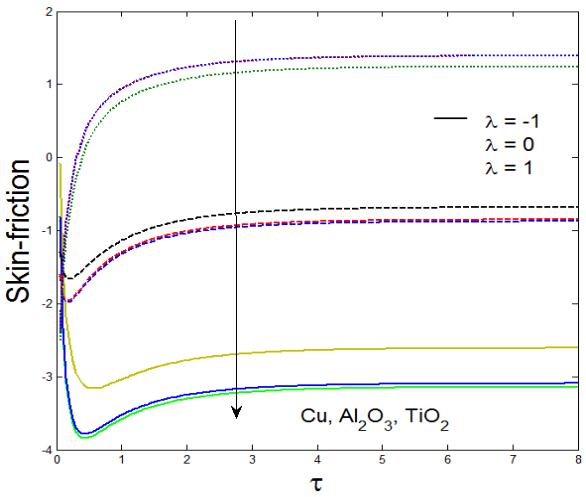

Figure 22. Skin friction for different nanoparticles when K=0.

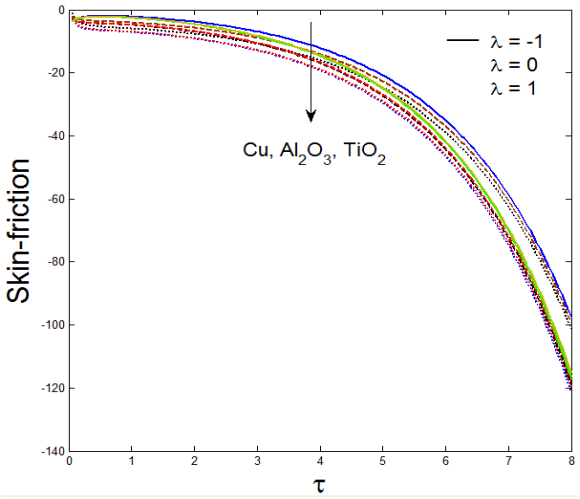

Figure 23. Skin friction for different nanoparticles when K=1.

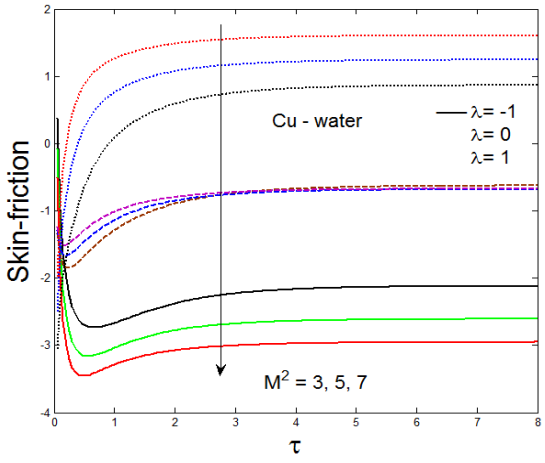

Figure 24. Skin friction for different M^2, when K=0.

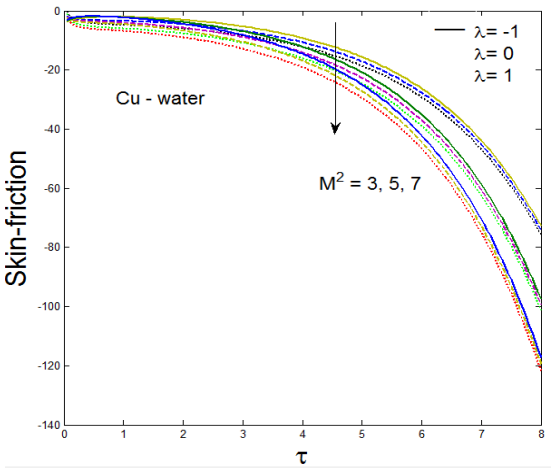

Figure 25. Skin friction for different M^2, when K=1.

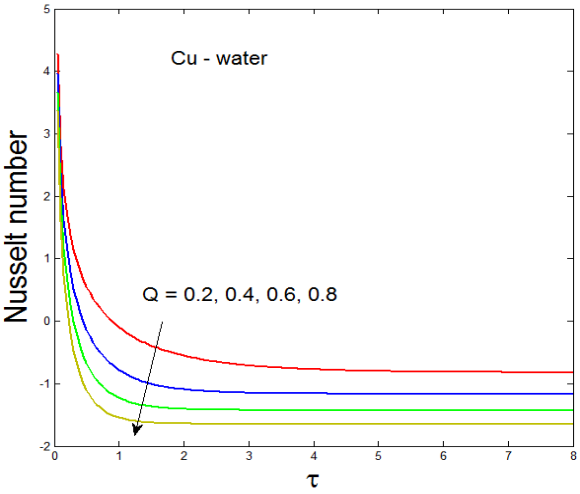

Figure 26. Nusselt number variation for different Q.

Table 1. Thermophysical properties of water and nanoparticles Oztop and Abu-Nada [54].

Physical properties	Water/ base fluid	Cu (copper)	Al_2O_3 (alumina)	TiO_2 (titanium Oxide)
ρ (kg/m^3)	997.1	8933	3970	4250
c_p (J/kg. K)	4179	385	765	686.2
k (W/m. K)	0.613	401	40	8.9538
$\beta \times 10^5$(K^{-1})	21	1.67	0.85	0.90
ϕ	0.0	0.05	0.15	0.2
σ (S/m)	5.5×10^{-6}	59.6×10^6	35×10^6	2.6×10^6

4. Conclusions

Natural conductive nanofluid flow past a rolling upright plate influenced by magnetic lines of force field when the magnetic intensity associated with the fluid or to the moving plate studied in duel case (i) when magnetic induction associated with the fluid (K=0) (ii) and the magnetic lines are being associated with moving upright plate (K=1). The dimensionless governing model involved in this study is tackled with the help of the method of integral transforms without any restriction. The numerical computations performed for plottings of fluid momentum, fluid temperature, heat flow rate, and friction drag closer to the plate are discussed: The velocity of the nanofluid decreases with increasing the magnetic parameter; An increased radiation parameter leads to fluid velocity in the boundary layer region; The velocity of the nanofluid increases with increasing heat source/sink; The temperature of the nanofluid increases with increasing radiation parameters; The temperature of the nanofluid decreases with increasing Prandtl number; The Nuselt number at the plate for Cu- water nanofluid increases with increasing radiation parameters; The Nuselt number at the plate for Cu- water nanofluid decreases with increasing radiation parameters; Skin friction at the plate for Cu- water nanofluid decreases with increasing magnetic parameters.

Funding

This research received no external funding

Acknowledgments

We are very much thankful to the reviewers for their valuable suggestions for improving the manuscript.

Conflicts of Interest

The authors declare no conflict of interest

References

1. Choi, U.S.; Eastman, J.A. Enhancing thermal conductivity of fluids with nanoparticles. *ASME International Mechanical Engineering Congress & Exposition* **1995**, San Francisco, CA, USA.
2. Eastman, J.A.; Choi, U.S.; Li, S.; Thompson, L.J.; Lee, S. Enhanced thermal conductivity through the development of nanofluids. *MRS Online Proceedings Library* **1996,** 457, 3-11.
3. Eastman, J.A.; Choi, U.S.; Li, S.; Yu, W.; Thompson, L.J. Anomalously increased effective thermal conductivities of ethylene glycol-based nanofluids containing copper nanoparticles. *Appl. Phys. Lett* **2001**, *78*, 718-720, https://doi.org/10.1063/1.1341218.

4. Choi, U.S.; Zhang, Z.G.; Yu, W.; Lockwood, F.E.; Grulke, E.A. Anomalous thermal conductivity enhancement in nanotube suspensions. *Appl. Phys. Lett.* **2001**, *79*, 2252-2254, https://doi.org/10.1063/1.1408272.
5. Das, S.K.; Putra, N.; Thiesen, P.; Roetzel, W. Temperature dependence of thermal conductivity enhancement for nanofluids. *J. Heat Transfer* **2003**, *125* , 567-574, https://doi.org/10.1115/1.1571080.
6. Keblinski, P.; Phillpot, S.R.; Choi, U.S.; Eastman, J.A. Mechanisms of heat flow in suspensions of nano-sized particles (nanofluids). *Int. J. Heat Mass Transfer* **2002**, *45*, 855-863, https://doi.org/10.1016/S0017-9310(01)00175-2.
7. Buongiorno, J.; Hu, W. Nanofluid coolants for advanced nuclear power plants. *Proceedings of ICAPP* **2005**,15-19.
8. Das, S.K.; Choi, U.S. A review of heat transfer in nanofluids. *Adv. Heat Transf* **2009**, *41*, 81-197, https://doi.org/10.1016/S0065-2717(08)41002-X.
9. Kakaç, S.; Pramuanjaroenkij, A. Review of convective heat transfer enhancement with nanofluids. *Int. J. Heat Mass Transf* **2009,** *52*, 3187-3196, https://doi.org/10.1016/j.ijheatmasstransfer.2009.02.006.
10. Wang, X.Q.; Mujumdar, A.S. Heat transfer characteristics of nanofluids: a review. *Int. J. Therm. Sci* **2007,** *46*, 1-19, http://dx.doi.org/10.1016/j.ijthermalsci.2006.06.010.
11. Sheikholeslami, M.; Ganji, D.D.; Rashidi, M.M. Ferrofluid flow and heat transfer in a semi annulus enclosure in the presence of magnetic source considering thermal radiation. *J Taiwan Inst Chem Eng* **2015**, *47*, 6-17, https://doi.org/10.1016/j.jtice.2014.09.026.
12. Sheikholeslami, M. Effect of uniform suction on nanofluid flow and heat transfer over a cylinder. *J Braz Soc Mech Sci Eng* **2015**, *37*, 1623-1633, http://dx.doi.org/10.1007/s40430-014-0242-z.
13. Kandelousi, M.S. KKL correlation for simulation of nanofluid flow and heat transfer in a permeable channel. *Phys. Lett. A* **2014,** *378*, 3331-3339, http://dx.doi.org/10.1016/j.physleta.2014.09.046.
14. Kuznetsov, A.V.; Nield, D.A. Natural convective boundary-layer flow of a nanofluid past a vertical plate. *Int. J. Therm. Sci* **2010,** *49*, 243-247, http://dx.doi.org/10.1016/j.ijthermalsci.2009.07.015.
15. Hamad, M.A.A.; Pop, I. Unsteady MHD free convection flow past a vertical permeable flat plate in a rotating frame of reference with constant heat source in a nanofluid. *Heat and Mass Transf* **2011**, *47*, 1517, http://dx.doi.org/10.1007/s00231-011-0816-6.
16. Hamad, M.A.A.; Pop, I.; Ismail, A.M. Magnetic field effects on free convection flow of a nanofluid past a vertical semi-infinite flat plate. *Nonlinear Anal.: Real World Appl* **2011**, *12*, 1338-1346, http://dx.doi.org/10.1016/j.nonrwa.2010.09.014.
17. Chamkha, A.J.; Aly, A.M. MHD free convection flow of a nanofluid past a vertical plate in the presence of heat generation or absorption effects. *Chem Eng Commun* **2010**, *198*, 425-441, http://dx.doi.org/10.1080/00986445.2010.520232.
18. Turkyilmazoglu, M.; Pop, I. Heat and mass transfer of unsteady natural convection flow of some nanofluids past a vertical infinite flat plate with radiation effect. *Int. J. Heat Mass Transf* **2013**, *59*, 167-171, http://dx.doi.org/10.1016/j.ijheatmasstransfer.2012.12.009.
19. Turkyilmazoglu, M. Unsteady convection flow of some nanofluids past a moving vertical flat plate with heat transfer. *J Heat Transfer* **2014**, *136*, 031704, http://dx.doi.org/10.1115/1.4025730.
20. Kumar, B.R.; Kumar, T.S.; Kumar, A.G. Thermal diffusion and radiation effects on unsteady free convection flow in the presence of magnetic field fixed relative to the fluid or to the plate. *Front. Heat Mass Transf* **2015**, *6*, http://dx.doi.org/10.5098/hmt.6.12.
21. Sheikholeslami, M.; Ganji, D.D.; Javed, M.Y.; Ellahi, R. Effect of thermal radiation on magnetohydrodynamics nanofluid flow and heat transfer by means of two phase model. *J. Magn. Magn. Mater* **2015**, *374*, 36-43, http://dx.doi.org/10.1016/j.jmmm.2014.08.021.
22. Sheikholeslami, M.; Bandpy, M.G.; Ellahi, R.; Zeeshan, A. Simulation of MHD CuO–water nanofluid flow and convective heat transfer considering Lorentz forces. *J. Magn. Magn. Mater* **2014**, *369*, 69-80, http://dx.doi.org/10.1016/j.jmmm.2014.06.017.
23. Sheikholeslami, M.; Gorji-Bandpy, M.; Ganji, D.D. Lattice Boltzmann method for MHD natural convection heat transfer using Nanofluid. *Powder Technol* **2014**, *254*, 82-93, https://doi.org/10.1016/j.powtec.2013.12.054.
24. Sheikholeslami, M.; Ganji, D.D. Unsteady nanofluid flow and heat transfer in presence of magnetic field considering thermal radiation. *J Braz Soc Mech Sci Eng* **2015**, *37*, 895-902, http://dx.doi.org/10.1007/s40430-014-0228-x.

25. Das, S.; Jana, R.N. Natural convective magneto-nanofluid flow and radiative heat transfer past a moving vertical plate. *Alex. Eng. J* **2015**, *54*, 55-64, http://dx.doi.org/10.1016/j.aej.2015.01.001.
26. Loganathan, P.; Nirmal Chand, P.; Ganesan, P. Transient natural convective flow of a nanofluid past a vertical plate in the presence of heat generation. *J. Appl. Mech. Tech. Phys* **2015**, *56*, 433-442, http://dx.doi.org/10.1134/s002189441503013x.
27. Singh, A.K. Effects of Heat Source/Sink and Radiative Heat Transfer on Hydromagnetic Natural Convective Flow Through a Vertical Channel. *Comput. Therm. Sci* **2010**, *2*, 323-332, http://dx.doi.org/10.1615/ComputThermalScien.v2.i4.30.
28. Rosseland, S. Astrophysik auf Atomtheoretischer Grundlagen. Springer-Verlag **1931**, Berlin, https://doi.org/10.1007/978-3-662-26679-3.
29. Mondal, P.; Mahapatra, T.R.; Parveen, R. Entropy generation in nanofluid flow due to double diffusive MHD mixed convection. *Heliyon* **2021**,*7*, e06143, https://doi.org/10.1016/j.heliyon.2021.e06143.
30. Abbas, N.; Shatanawi, W; Abodayeh, K. Computational Analysis of MHD Nonlinear Radiation Casson Hybrid Nanofluid Flow at Vertical Stretching Sheet. *Symmetry* **2022**, *14*, 1494, https://doi.org/10.3390/sym14071494.
31. Chen, J.; Chen, W.; Selim, M.M. Numerical simulation of nanofluid transportation due to MHD within a porous space. *Appl. Nanosci* **2021**, https://doi.org/10.1007/s13204-021-01988-0.
32. Zainal, N.A.; Nazar, R.; Naganthran, K.; Pop, I. Stability analysis of unsteady MHD rear stagnation point flow of hybrid nanofluid. *J.Math* **2021**, *9*, 2428, https://doi.org/10.3390/math9192428.
33. Rehman, A.; Salleh, Z. Approximate analytical analysis of unsteady MHD mixed flow of non-Newtonian hybrid nanofluid over a stretching surface. *Fluids* **2021**, *6*, 138, https://doi.org/10.3390/fluids6040138.
34. Teh, Y.Y.; Ashgar, A. Three dimensional MHD hybrid nanofluid Flow with rotating stretching/shrinking sheet and Joule heating. *CFD Lett* **2021**, *13*, 1-19, https://doi.org/10.37934/cfdl.13.8.119.
35. Habib, D.; Salamat, N.; Abdal, S.; Siddique, I.; Salimi, M.; Ahmadian, A. On time dependent MHD nanofluid dynamics due to enlarging sheet with bioconvection and two thermal boundary conditions. *Microfluidic Nanofluidics* **2022**, *26*, 11, https://doi.org/10.1007/s10404-021-02514-y.
36. Gürdal, M.; Pazarlıoğlu, H.K.; Tekir, M.; Arslan, K.; Gedik, E. Numerical investigation on turbulent flow and heat transfer characteristics of ferro-nanofluid flowing in dimpled tube under magnetic field effect. *Appl. Therm. Eng* **2022**, *200*, 117655, https://doi.org/10.1016/j.applthermaleng.2021.117655.
37. Usafzai, W.K.; Aly, E.H.; Alshomrani, A.S.; Ullah, M.Z. Multiple solutions for nanofluids flow and heat transfer in porous medium with velocity slip and temperature jump. *Int. Commun. Heat Mass Transf* **2022** , *131*, 105831, https://doi.org/10.1016/j.icheatmasstransfer.2021.105831.
38. Bilal, M.; Gul, T.; Alsubie, A.; Ali, I. Axisymmetric hybrid nanofluid flow with heat and mass transfer amongst the two gyrating plates. *Z Angew Math Mech* **2021**, *101*, e202000146, https://doi.org/10.1002/zamm.202000146.
39. Gouran, S.; Mohsenian, S.; Ghasemi, S.E. Theoretical analysis on MHD nanofluid flow between two concentric cylinders using efficient computational techniques. *Alex. Eng. J* **2022 ,** *61*, 3237-3248, https://doi.org/10.1016/j.aej.2021.08.047.
40. Soomro, F.A.; Usman, M.; El-Sapa, S.; Hamid, M.; Haq, R.U. Numerical study of heat transfer performance of MHD Al2O3-Cu/water hybrid nanofluid flow over inclined surface. *Arch. Appl. Mech* **2022,** *92*, 2757-2765, https://doi.org/10.1007/s00419-022-02214-1.
41. Ali, L.; Ali, B.; Ghori, M.B. Melting effect on Cattaneo–Christov and thermal radiation features for aligned MHD nanofluid flow comprising microorganisms to leading edge: FEM approach. *Comput. Math. with Appl* **2022**, *109*, 260-269, https://doi.org/10.1016/j.camwa.2022.01.009.
42. Asjad, M.I.; Sarwar, N.; Ali, B.; Hussain, S.; Sitthiwirattham, T.; Reunsumrit, J. Impact of Bioconvection and Chemical Reaction on MHD Nanofluid Flow Due to Exponential Stretching Sheet. *Symmetry* **2021**, *13*, 2334, https://doi.org/10.3390/sym13122334.
43. Li, Y.X.; Mishra, S.R.; Pattnaik, P.K.; Baag, S.; Li, Y.M.; Khan, M.I.; Khan, N.B.; Alaoui, M.K.; Khan, S.U. Numerical treatment of time dependent magnetohydrodynamic nanofluid flow of mass and heat transport subject to chemical reaction and heat source. *Alex. Eng. J.* **2022** *61*, 2484-2491, https://doi.org/10.1016/j.aej.2021.07.030.
44. Arulmozhi, S.; Sukkiramathi, K.; Santra, S.S.; Edwan, R.; Fernandez-Gamiz, U.; Noeiaghdam, S. Heat and mass transfer analysis of radiative and chemical reactive effects on MHD Nanofluid over an infinite movingverticalplate. *Results in Engineering* **2022**, *14*, 100394, https://doi.org/10.1016/j.rineng.2022.100394.

45. Nagaraja, B.; Gireesha, B.J.; Soumya, D.O.; Almeida, F. Characterization of MHD convective flow of Jeffrey nanofluid driven by a curved stretching surface by employing Darcy–Forchheimer law of porosity. *Waves Random Complex Media* **2022**, *32*, 1-20, https://doi.org/10.1080/17455030.2021.2020933.
46. Hossain, R.; Azad, A.K.; Jahid Hasan, M.; Rahman, M.M. Radiation effect on unsteady MHD mixed convection of kerosene oil-based CNT nanofluid using finite element analysis. *Alex. Eng. J* **2022**, *61*, 8525-8543, https://doi.org/10.1016/j.aej.2022.02.005.
47. Siddiqui, B.K.; Batool, S.; ul Hassan, Q.M.; Malik, M.Y. Irreversibility analysis in the boundary layer MHD two dimensional flow of Maxwell nanofluid over a melting surface. *Ain Shams Eng. J* **2021**, *12*, 3217-3227, https://doi.org/10.1016/j.asej.2021.01.017.
48. Al-Farhany, K.; Abdulkadhim, A.; Hamzah, H.K.; Ali, F.H.; Chamkha, A. MHD effects on natural convection in a U-shaped enclosure filled with nanofluid-saturated porous media with two baffles. *Prog. Nucl. Energy* **2022**, *145*, 104136, https://doi.org/10.1016/j.pnucene.2022.104136.
49. Hosseinzadeh, K.; Mogharrebi, A.R.; Asadi, A.; Sheikhshahrokhdehkordi, M.; Mousavisani, S.; Ganji, D.D. Entropy generation analysis of mixture nanofluid ($H_2O/c_2H_6O_2$)–Fe_3O_4 flow between two stretching rotating disks under the effect of MHD and nonlinear thermal radiation. *Int. J. Ambient Energy* **2022**, *43*, 1045-1057, https://doi.org/10.1080/01430750.2019.1681294.
50. Habib, D.; Salamat, N.; Abdal, S.H.S.; Ali, B. Numerical investigation for MHD Prandtl nanofluid transportation due to a moving wedge: Keller box approach. *Int. Commun. Heat Mass Transf* **2022**, *135*, 106141, https://doi.org/10.1016/j.icheatmasstransfer.2022.106141.
51. Cramer, K.R., Pai, S.I. *Magnetofluid dynamics for engineers and applied physicists*. McGraw-Hill **1973**, New York.
52. Raptis, A.; Singh, A.K. MHD free convection flow past an accelerated vertical plate. *Int. Commun. Heat Mass Transf* **1983**, *10*, 313-321, https://doi.org/10.1016/0735-1933(83)90016-7.
53. Tokis, J.N. A class of exact solutions of the unsteady magnetohydrodynamic free-convection flows. *Astrophys. Space Sci* **1985**, *112*, 413-422, http://dx.doi.org/10.1007/bf00653524.
54. Oztop, H.F.; Abu-Nada, E. Numerical study of natural convection in partially heated rectangular enclosures filled with nanofluids. *Int J Heat Fluid Flow* **2008**, *29*, 1326-1336, http://dx.doi.org/10.1016/j.ijheatfluidflow.2008.04.009.